Konrad-Zuse-Zentrum für Informationstechnik Berlin
Heilbronner Str. 10, D-10711 Berlin - Wilmersdorf

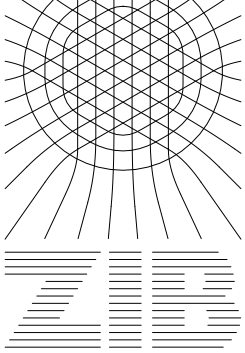

Jochen Fröhlich, Kai Schneider

An adaptive Wavelet–Vaguelette Algorithm for the Solution of Nonlinear PDEs

Preprint SC 95-28 (November 1995)

Contents

An adaptive Wavelet–Vaguelette Algorithm for the Solution of Nonlinear PDEs

Jochen Fröhlich *, Kai Schneider †

Abstract

The paper describes a fast algorithm for the discrete periodic wavelet transform and its inverse without using the scaling function. The approach permits to compute the decomposition of a function into a lacunary wavelet basis, i.e. a basis constituted of a subset of all basis functions up to a certain scale, without modification. The construction is then extended to operator–adapted biorthogonal wavelets. This is relevant for the solution of non–linear evolutionary PDEs where a priori information about the significant coefficients is available. We pursue the approach described in [FS94] which is based on the explicit computation of the scalewise contributions of the approximated function to the values at points of hierarchical grids. Here, we present an improved construction employing the cardinal function of the multiresolution. The new method is applied to the Helmholtz equation and illustrated by comparative numerical results. It is then extended for the solution of a nonlinear parabolic PDE with semi–implicit discretization in time and self–adaptive wavelet discretization in space. Results with full adaptivity of the spatial wavelet discretization are presented for a one–dimensional flame front as well as for a two–dimensional problem.

Key Words: Wavelets, Adaptive PDE Methods, Reacting Flows

AMSMOS, MSC 1991 subject classification:
Primary 65M60; Secondary 80A32, 76V05.

*Konrad–Zuse–Zentrum Berlin, Heilbronner Str. 10, D-10711 Berlin-Wilmersdorf, Germany. froehlich@zib-berlin.de

†Fachbereich Chemie – Technische Chemie Universität Kaiserslautern, D-67663 Kaiserslautern, Germany. kschneid@rhrk.uni-kl.de

1 Introduction

In recent years the development of multiresolution techniques and wavelets has had a tremendous impact on signal and image processing and many other fields. One of them is the numerical solution of partial differential equations where related ideas have been popular for a long time. It is beyond the scope of this introduction to survey all the relevant literature on this subject in detail. A recent attempt has been made by Jawerth and Sweldens [JS94] to which the reader is refered for more comparative information.

The currently existing algorithms that employ a wavelet basis for the solution of PDEs can, very roughly, be divided in two categories. The first ones use the localization of the wavelets in space and frequency for the representation of operators by means of sparse matrices [Jaf92, BCR91] which is discussed in [Mey90] from a theoretical point of view. This results in efficient multilevel preconditioners for the iterative solution of the resulting linear systems, e.g. [DK92]. A regular fine grid is generally still present in this class of methods so that they are close to the multigrid philosophy. Although we have only cited relatively few references here, the majority of the present wavelet methods falls into this category.

The second approach, which is also adopted in the present paper, employs an adaptively selected set of wavelet basis functions to represent the solution of the PDE [LT90, MPR91, MR92, BMP92]. Apart from using the above localization properties this aims at savings by adapting the set of basis functions according to the actual shape of the solution, a strategy similar to adaptive hierarchical finite elements [DLY89]. The present algorithm is direct. It avoids the solution of any linear system by diagonalizing the stiffness matrix through an appropriate choice of test and trial functions in a Petrov–Galerkin method. The approach exploits the compression property, similarly as a wavelet analysis of a signal. In contrast to most signal processing tasks, however, avoiding a costly regular fine grid for the solution of a PDE requires a bottom–up strategy of successive local refinements. Only the subset of the relevant amplitudes is to be computed. This loss of regularity in the index set is an essential difficulty of the approach which we overcome in a particular way in the present paper. Recall that the classical Mallat algorithm can no longer be employed in the lacunary case as it is based on the use of the scaling functions' coefficients on each scale which do not exhibit the same lacunarity as the wavelet coefficients. In that case it is not clear how to define a suitable projection on the lacunary basis.

Let us note that the need of repeated transforms between physical space, i.e. the values at certain grid points and coefficient space, originates in the nonlinearity of the PDE to be solved. For linear operations such as derivation, multiplication by powers of the independent variable etc. the conversion to operations on the wavelet coefficients is possible [Lem91, EOZ94]. For simple nonlinearities the approximate evalution in coefficient space has been studied by Beylkin [Bey93] and others. But for general nonlinear terms such as encountered in combustion modelling the evalutation in physical space seems to be unavoidable.

Different strategies to cope with locally refined wavelet basis have been developed. Plantevin [Pla92] constructs an orthonormal basis for a given locally refined dyadic grid. As each modification of the grid requires a new basis construction this can become very costly and seems not to be appropriate for the use in the adaptive discretization of unsteady solutions of PDEs. Ponenti [Pon94] aims at retaining as much of the unmodified compactly supported wavelet basis as possible and succeeds in modifying only those functions that live near the border of the index set of retained wavelets. However, the projection step onto the space spanned by these functions is left unconsidered. Sweldens [Swe94] has developed a strategy which allows almost arbitrary spacing of grid points. A completly irregular discretization however makes it difficult to take into account differential operators and to consider smooth bases.

The present construction retains the wavelet basis as it is. A lacunary subset is accessed through a simple hierarchical subtraction strategy which permits to compute individual coefficients of the wavelet series with linear operation count [FS94].

In the first part of the paper we start with a detailed description of the algorithm for a pure wavelet decomposition and improve the former algorithm by employing the cardinal Lagrange function. This is important as it results in speed up, facilitates the implementation, and allows a clearer analysis of the procedure. Up to here, the approach is similar to the partial collocation method briefly sketched in [MR92] and the multilevel collocation for frames of [VPS95].

The next important step is to incorporate the differential operator into the basis as first proposed in [Tch87] and employed in [LT90]. Thereby, the related stiffness matrix is diagonalized avoiding its assembly and inversion. This is particularly favorable when frequently changing the set of active basis functions. We show how the hierarchical decomposition into a lacunary basis of the first step can be adapted to this situation. Thereby, we arrive at an interpolatory transform for a fully adaptive operator–orthogonal wavelet–vaguelette decomposition. It is implemented to solve elliptic problems in one and two space dimensions.

In a final step the algorithm is applied to unsteady reaction–diffusion problems where the semi–implicit time discretization requires the solution of an elliptic problem in each time step. The set of relevant coefficients to be computed is furnished by an adaption strategy in coefficient space. Note that different boundary conditions can be applied in a later stage by means of an imbedding strategy such as proposed by [QW93, GRWZ93].

The paper is organized as follows. We start in Section 2 with the case of a pure wavelet decomposition. This permits to introduce the relevant notation and properties. Furthermore, the inverse transform described here will be retained later on in the complete algorithm. In Section 3 we develop the wavelet–vaguelette decomposition and demonstrate its relation to PDEs. For clearness and ease of notation the method is outlined in these first sections considering the real line. The practical implementation, however, makes use of periodicity. Hence assembling some remarks related to this topic in a separate section seems to be appropriate (Section 4). With the ground prepared in such a way the description of the two–dimensional algorithm in Section 5 can be rather brief.

In Section 6 we investigate the essential decay properties of the employed basis function by means of numerical experiments. We finally report sample computations for one– and two–dimensional flames which illustrate the properties of the presented method.

2 Recursive interpolatory transform for orthogonal wavelets

The following approach is by no means restricted to orthonormal wavelets but can rather be applied to any basis exhibiting scale separation (even when this only holds in a qualitative way as in [BFF95]). Since orthogonality of the employed basic wavelets is crucial for the later discretization of a PDE we formulate it in these terms right from the beginning.

2.1 Multiresolution and interpolation

Assume the set of closed subspaces $\{V_j\}_{j\in\mathbb{Z}}$ with $V_j \subset V_{j+1}$ being a multiresolution analysis (MRA) of $L^2(\mathbb{R})$. Let it be generated by some function $b(x)$ through dyadic dilation and translation, i.e.

$$b_{j,k}(x) = 2^{j/2}\, b(2^j x - k) \quad , \qquad b_j = b_{j,0} \tag{2.1}$$

with $\{b_{j,i}\}_i$ constituting a Riesz basis of V_j, not necessarily being orthogonal. The index convention for other functions below will often be slightly different from (2.1) but made precise each time. Dropping the second index for zero shift is used throughout. The orthonormal scaling function and wavelet function for this MRA are denoted ϕ and ψ, respectively. The function ϕ can be obtained from b through orthonormalization, but occasionally we also set $b = \phi$ right from the start. Furthermore, we suppose that ψ has $M + 1$ vanishing moments. Due to the MRA–structure any function $f_J \in V_J$ can be written as

$$f_J(x) \;=\; \sum_k c_{J,k}\; \phi_{J,k}(x) \;=\; \sum_k c_{0,k}\; \phi_{0,k}(x) \;+\; \sum_{j=0}^{J-1} \sum_k \; d_{j,k}\; \psi_{j,k}(x) \tag{2.2}$$

employing (2.1) for the definition of shift and scale index. Bounds for the translation indices are left unspecified throughout as these will later be governed by the periodization. The scale index $j = 0$ in (2.2) is arbitrary and chosen for later convenience. The filters

$$G_n^j = \langle \phi_{j,n}, \psi_{j-1,0} \rangle \;, \qquad H_n^j = \langle \phi_{j,n}, \phi_{j-1,0} \rangle \tag{2.3}$$

are classically used for the transition between both representations. They can be obtained in physical space for compactly supported bases and in Fourier space through

$$\widehat{H}^*(\omega) = \widehat{\phi}(2\omega)/\widehat{\phi}(\omega) \quad , \qquad \widehat{G}^*(\omega) = \widehat{\psi}(2\omega)/\widehat{\phi}(\omega) \tag{2.4}$$

where the notation of (8.5) is employed to emphasize the periodicity of these expressions with respect ot ω. Given a function $f \in L^2(\mathbb{R})$, a projection P_J has to be applied to get $f_J = P_J f$. At this point there exists a certain liberty. In [SP94] different quadrature formulas are developed for this task. The algorithms below rely on the collocation projection as it allows for easy connection to values in physical space and for successive coarsening of the employed grids. It is defined by

$$f_J(\frac{k}{2^J}) = f(\frac{k}{2^J}) \tag{2.5}$$

Hence, f_J in (2.2) is determined through

$$f_J(x) = \sum_k f(\frac{k}{2^J})\ S_J(x - \frac{k}{2^J}) \tag{2.6}$$

with the cardinal Lagrange function S_J of V_J defined by

$$S_J(\frac{i}{2^J}) = \delta_{i,0} \quad , \qquad V_J = \overline{span}\{S_{J,k} = S_J(x - \frac{k}{2^J})\}_k \tag{2.7}$$

(The scale index for this function is defined without the factor $2^{j/2}$ for ease of notation.) Combining (2.2) and (2.6), the coefficients $c_{J,k}$ in (2.2) are computed by application of the interpolation filter

$$I_n^J = \langle S_{J,n}, \phi_{J,0} \rangle\ , \quad \widehat{I^J} = 2^{-3J/2}\ \widehat{I}(\frac{\omega}{2^j})\ , \quad \widehat{I}^*(\omega) = \widehat{S}(\omega)/\widehat{\phi}(\omega) \tag{2.8}$$

to the sampled values $\{f(\frac{k}{2^J})\}_k$.

Note that when using wavelets for the discretization of a PDE one would like to exploit the regularity of these functions to obtain efficient approximation of smooth functions. If, however, the projection step has a truncation error of order much lower than this regularity, it is useless to employ regular wavelets. The classical projection $c_{J,i} = f(x_{J,i})$ to determine f_J in (2.2), for example, converges only like $O(h)$ with $h = 2^{-J}$.

Let us remark that in the L^2 setting considered so far interpolation has no meaning. However, as soon as the basis functions have sufficient regularity the same multiresolution can be viewed as a multiresolution in H^r, $(r \geq 1)$ without any further change [BN93].

The existence of a cardinal Lagrange function S_J of V_J is guaranteed by

THEOREM 1. *[Wal92] For a reproducing kernel Hilbert space V spanned by a Riesz basis $\{b(x-k)\}_{k\in\mathbb{Z}}$ such that $\widehat{b}^*(\omega) \neq 0$, a cardinal Lagrange function exists and is given by*

$$\widehat{S}(\omega) = \frac{\widehat{b}(\omega)}{\widehat{b}^*(\omega)} \quad , \qquad \omega \in \mathbb{R} \tag{2.9}$$

Remark: In [Wal92] the assertion is first proved for $b = \phi$ constituting the kernel of the reproducing kernel Hilbert space V. Eq. (2.9) then is deduced as Riesz bases can be converted from one into the other and S is unique modulo discrete shifts. For spline spaces this equation has already been used by Schoenberg [Sch69].

2.2 Recursive interpolatory transform

Consider the points of nested dyadic grids in $\mathbb{R}$

$$x_{j,i} = \frac{i}{2^j} \quad , \qquad i, j \in \mathbb{Z} \tag{2.10}$$

verifying the trivial recursion

$$x_{j+1,2i} = x_{j,i} \qquad , \qquad x_{j+1,2i+1} = \tfrac{1}{2} x_{j,i} + \tfrac{1}{2} x_{j,i+1} \tag{2.11}$$

In the following the cardinal interpolation function will play the role of the scaling function employed in the classical algorithm. We therefore define the filters

$$D_m^{j,j-1} = \langle S_{j,m}, \psi_{j-1,0} \rangle \tag{2.12}$$

representing collocation projection onto V_j and subsequent projection onto W_{j-1} when applied to the values $\{f(x_{j,i})\}_i$. In the sequel $D_m^j = D_m^{j,j-1}$ for conciseness.
Similar to recursions in j for $\widehat{H^j}, \widehat{G^j}$ one can show

THEOREM 2. *The filters D^j in (2.12) verify the recurrence relation*

$$(\widehat{D^{j-1}})_k = 2^{3/2} (\widehat{D^j})_{2k} \tag{2.13}$$

Proof. Equations (2.3), (2.8), (2.12) yield

$$D_m^j = \sum_l G_l^j \; I_{l-m}^j$$

Transfer to Fourier space and application of (2.4) and (2.8) back and forth for $j-1$ and j, respectively, gives the assertion. □
The following theorem describes the biorthogonality of the sampled wavelets and D^J.

THEOREM 3. *Given ψ_{ji} and D_n^J defined by (2.12)*

$$\sum_n D_{n-2k}^J \; \psi_{j,l}(\frac{n}{2^J}) = \delta_{j,J-1} \; \delta_{l,k} \quad , \qquad j < J \tag{2.14}$$

Proof. The sampling theorem in V_J yields

$$\psi_{j,l}(x) = \sum_n \psi_{j,l}(\frac{n}{2^J}) \; S_{J,n}(x) \quad , \qquad j < J \tag{2.15}$$

Applying scalar products with $\psi_{J-1,k}$ on both sides and using (2.12), together with the orthogonality of the wavelets proves (2.14). □

COROLLARY 1.

$$\sum_n n^k \; D_n^j = 0 \quad , \qquad k = 0, \ldots, M \quad , \qquad j \in \mathbb{Z} \tag{2.16}$$

Proof. Equation (2.16) follows from (2.15) with $\psi(x)$ replaced by x^k. Scalar products with $\psi_{J-1,k}$ on both sides allow to use the moment conditions for ψ. □

The above shows that in fact the filters D^j correspond to finite difference formulas of order $M+1$. With the present construction these filters do generally not have compact support which results in most cases from the appearance of the cardinal function. In particular, their decay is algebraic for the multiresolutions of Meyer wavelets employed below and exponential for Spline wavelets. The latter also holds for Daubechies wavelets since their cardinal function has non–compact support (except the Haar case) and decays exponentially [Wal92].

Up to now we have used the filter D^j only with $j = J$. The following algorithm accomplishes a wavelet transform by successively coarsening the samples.

Algorithm 1: Wavelet transform

given samples $\{f(x_{J,i})\}_i$ for some $J \in \mathbb{N}$ with $x_{J,i}$ from (2.10).

step 0 $f_J(x_{J,i}) = f(x_{J,i})$, set $j = J$.

step 1 Compute

$$d_{j-1,k} = \sum_n f_j(x_{j,n}) \; D_{n-2k}^j \quad , \qquad k = \ldots \tag{2.17}$$

step 2 Substract the contribution from W_{j-1} at the even grid points

$$f_{j-1}(x_{j-1,i}) = f_j(x_{j,2i}) \; - \sum_k d_{j-1,k} \; \psi_{j-1,k}(x_{j-1,i}) \; , \qquad i = \ldots \tag{2.18}$$

iterate step 1 and step 2 down to $j = 0$.

finally Compute $\{c_{0,i}\}_i$ using $\{I_n^0\}_n$ from (2.8).

The algorithm exploits the fact that if f_j is known to belong to V_j, the values at the points $x_{j,i}$ uniquely determine the decomposition in this space by the sampling theorem. In the periodic case the algorithm even becomes slightly simpler as the final step almost disappears. If furthermore the entire set of coefficients in (2.2) is to be computed, it is more economical to use fast convolution by means of FFT employing the technique described in [FS94]. But this is not the aim here as we consider non–uniform discretization.

2.3 Inverse transform

Similar to the above algorithm we can now devise an inverse transform based on the following relation.

THEOREM 4. *With $S_{j,i}$ and D_n^j from (2.7) and (2.12), respectively,*

$$\sum_i S_{j-1,k}(x_{j,i})\; D^j_{i-2k} \;= 0 \tag{2.19}$$

Proof. Analogeously to Theorem 3, equation (2.19) is proved starting from

$$S_{j-1,k}(x) = \sum_i S_{j-1,k}(x_{j,i})\; S_{j,i}(x)$$

□

The resulting algorithm reads as follows

Algorithm 2: Inverse wavelet transform

given coefficients $\{c_{0,i}\}_i$, $\{d_{j,i}\}_{j=0,\ldots,J-1\,,\,i}$.

step 0 Set $j = 0$ and

$$f_0(x_{0,i}) = \sum_k c_{0,k}\,\phi_{0,k}(x_{0,i})$$

step 1 Compute f_{j+1} at even grid points

$$f_{j+1}(x_{j+1,2i}) = f_j(x_{j,i}) + \sum_k d_{j,k}\psi_{j,k}(x_{j,i}) \quad , \quad i = \ldots \tag{2.20}$$

step 2 Compute f_{j+1} at odd grid points,

$$f_{j+1}(x_{j+1,2i+1}) = \sum_k f_j(x_{j,k})S_{j,k}(x_{j+1,2i+1}) \;+\; \sum_k d_{j,k}\psi_{j,k}(x_{j+1,2i+1}) \quad , \quad i = \ldots \tag{2.21}$$

iterate step 1 and step 2 for $j = 1, \ldots, J-1$.

Using (2.7) and (2.11) step 1 and 2 can be assembled in

$$f_{j+1}(x_{j+1,i}) = \sum_k f_j(x_{j,k})S_{j,k}(x_{j+1,i}) \;+\; \sum_k d_{j,k}\psi_{j,k}(x_{j+1,i}) \quad , \quad i = \ldots \tag{2.22}$$

which again makes obvious the role of the cardinal function as a substitute for the scaling function.

2.4 Transform for a lacunary basis

In many applications a priori information can be used for adapting the index set of required coefficients in (2.2) to a given function f. In most cases local importance of fine scale coefficients is due to the presence of singularities or almost–singularities in f. The decay of the wavelet coefficients in scale and space depends on the strength of the singularity and is well known, see [Jaf89, Mey90] and others. Then, the relevant indices for $d_{j,i}$ fulfil a so-called cone condition. It roughly means that at a given point x with finest local scale j_x all basis functions on scales $j < j_x$ of which the (numerical) support contains x are retained. This property is no prerequisite for the sequel but increases the efficiency of the method.

Although generally having non–compact support the filters $D^j, \psi_{j,i}$ exhibit rapid decay and can therefore be truncated in space up to some prescribed tolerance. The operations in step 1 and step 2 of Algorithm 1 then are only carried out on subgrids of $\{x_{j,i}\}_i$. This increases savings in each step and requires f to be known only at the union of the involved truncated grids. At the price of a slight error, appart from the one due to the neglection of small coefficients, it yields an $O(N)$ operation count where N is the number of employed basis functions. The operation count for the inverse transform is the same as for Algorithm 1 since the sums in (2.21) are shorter than the one in (2.17). Observe that the error from truncation of the filters does not affect the perfect reconstruction property of the transform and its inverse which is preserved by construction. This was not necessarily the case in [FS94] where furthermore a grid finer than $\{x_{j,i}\}_i$ was required for the computation of $\{d_{j-1,i}\}_i$ to avoid aliasing. As a consequence, the restriction to wavelets well localized in Fourier space such as the Meyer wavelets is removed by the present method.

3 Operator-adapted bases

An essential step is now the extension of Algorithm 1 to biorthogonal vaguelettes. These can be adapted to certain operators so that such an algorithm may be applied to solve (pseudo–) differential or integral equations by a Petrov–Galerkin scheme. The result is a so–called wavelet–vaguelette decomposition of solution and right hand side introduced by Tchamitchian [Tch87]. Although wavelets are employed to furnish better bases for numerical algorithms than trigonometric polynomials the analysis below heavily relies on the Fourier transform. This technique is well suited for the considered operators and furnishes powerfull tools.

3.1 Biorthogonal vaguelettes

Let us denote by $\sigma(x,\xi) = \sum_{m=0}^{s} a_m(x)\ (2\pi i\,\xi)^m$ the symbol of a linear operator L of order $s \in \mathbb{N}_0$ given by $Lu = \sum_{m=0}^{s} a_m(x)\ (\partial_x)^m u(x)$. In the following we consider inhomogeneous elliptic differential operators with constant coefficients characterized by

$\sigma(x,\xi) = \sigma(\xi) > 0$ and aim to solve the equation

$$L\, u = f \tag{3.1}$$

for $u(x)$. The inverse L^{-1} is represented by the symbol $1/\sigma(\xi)$ and the adjoint L^* by the complex conjugate $\overline{\sigma(\xi)}$. The corresponding homogeneous operator which is obtained by only retaining the highest order term of L is denoted $\dot{L}$ with symbol $\dot{\sigma} = a_s\, \xi^s$.

Under suitable conditions (cf. below) one can define the functions

$$\theta_{j,i} = (L^*)^{-1}\, \psi_{j,i}\ , \quad \mu_{j,i} = L\, \psi_{j,i} \tag{3.2}$$

$$\eta_{j,i} = (L^*)^{-1}\, \phi_{j,i}\ , \quad \nu_{j,i} = L\, \phi_{j,i} \tag{3.3}$$

By construction these fulfill the bi–orthogonality relations

$$\langle \theta_{j,i}, \mu_{k,m} \rangle = \delta_{jk}\ \delta_{im}\ , \quad \langle \eta_{j,i}, \nu_{j,k} \rangle = \delta_{ik} \tag{3.4}$$

Observe that scale invariance (2.1) no longer holds. Apart from a scaling factor depending on s the reason is that an inhomogeneous operator (in contrast to a homogeneous one) involves spatial scales on its own determined by the ratios of different coefficients. These ratios are not altered with j in (3.2),(3.3). The functions $\theta_{j,i}, \mu_{ji}$ are called vaguelettes [Mey90] as they have similar properties as wavelets (not necessarily being orthogonal) apart from dilation invariance. In particular, they have vanishing moments and fast decay which is shown below. The latter property is of primary concern since it affects the length of the involved filters in the proposed method.

As $\lim_{j\to\infty} L\psi_{j,i} = \dot{L}\psi_{j,i}$ the homogeneous operator in some sense constitutes a worst case limit of L. We now analyse the functions in (3.2),(3.3) as well as the required operator–adapted cardinal functions. Replacing L with its homogeneous counterpart permits to verify that for $j \to \infty$, i.e. for strong refinement, no degradation occurs.

Let us start with the following statement which can be deduced from classical Fourier analysis [SW71]. It determines the decay of a function in physical space by the regularity of its Fourier transform.

THEOREM 5. *Let*

$$(d_\omega)^k\, \widehat{f} \in L^1(I\!R), \qquad k = 0, \ldots, n \tag{3.5}$$

for some $n \in I\!N_0$, possibly $k \in I\!N_0$.
Then $x^n f \in L^\infty(I\!R)$. This yields (Riemann-Lebesque)

$$\lim_{|x|\to\infty} x^n\, f = 0 \tag{3.6}$$

A priori, the Fourier transform in (3.5) has to be understood in a distributional sense. However, in all applications below the considered expressions belong to $L^2(I\!R)$ as well (without being mentioned explicitly every time) so that $\widehat{f}$ has the classical L^2–meaning. Theorem 5 can now be applied to the functions defined above.

THEOREM 6. *Let L be an inhomogeneous elliptic operator of order $s \in \mathbb{N}$ with symbol $\sigma > 0$. Let $\dot{L}$ be the corresponding homogeneous operator containing only the highest order term of L. Consider an MRA with the orthogonal wavelet ψ fulfilling*

$$| d_\omega^k \widehat{\psi}(\omega) | \leq \frac{C_k}{(1+ | \omega |)^{r+1+\epsilon}} \qquad k = 0, \ldots, n, \quad n \in \mathbb{N}_0 \tag{3.7}$$

for some $r \geq s$, $\epsilon > 0$ and positive constants C_k. Suppose further that

$$\int x^l \psi(x)\, dx = 0 \qquad l = 0, \ldots, M \tag{3.8}$$

with $M \geq s$.

Then the functions θ, μ, η, ν as defined in (3.2),(3.3) ($j = i = 0$) have the same asymptotic decay rate as ϕ and ψ. This remains true for θ, μ, ν when replacing the inhomogeneous operator by the homogeneous one.

Before turning to the proof a few remarks are appropriate. It will become clear that the above assumptions are no necessary conditions for the required decay rates but rather sufficient ones. They are oriented towards the typical MRAs and well suited for the present examples.

An r–regular MRA as defined by [Mey90] is a special case of the considered MRAs and is obtained for $k \in \mathbb{N}_0$ in (3.7). The above setting partly results from the desire to cover Meyer wavelets which need not be r–regular. Let us sum up the different parameters characterise the MRA: r determines the differentiability of ϕ and ψ, M specifies the number of vanishing moments, and n describes the decay of ϕ, ψ and their derivatives up to order r. For particular MRAs these parameters are coupled differently. The Meyer MRA corresponds to infinite r and infinite M while n depends on the construction ($n = 4$ in the present computations). Spline wavelets are related to $r = m - 1, M = m - 1$ and infinite n, where m denotes the (even) order of the spline.

Proof. Equation (3.7) yields

$$d_\omega^k \widehat{\psi}(\omega) \in L^1(\mathbb{R}) \qquad k = 0, \ldots, n \tag{3.9}$$

Hence from Theorem 5

$$| \psi(x) | \leq \frac{C}{(1+ | x |)^n} \tag{3.10}$$

for some positive C.

As the wavelet and the orthogonal scaling function are intimately related by construction, (3.7) and therefore (3.10) apply for ϕ as well.

Obviously, the power r is not required in the above. It serves however to prove the same decay for the derivatives in space $d_x^k \phi$ and $d_x^k \psi$ up to $k = r$ as these are reflected by multiplication with ω^k in Fourier space. Hence, ν and μ which are just sums of

derivatives up to order $s \leq r$ decay similarly to (3.10). This is not modified when replacing L with $\dot{L}$.

Let us now consider θ defined by $\widehat{\theta} = \widehat{\psi}/\overline{\sigma}$. The existence of the derivatives of $\widehat{\psi}$ up to $k = n$ and $\sigma \in C^\infty, \sigma > 0$ show that $d_\omega^k \widehat{\theta}, k = 0, \ldots, n$ exist. For small ω the symbol tends to a constant while $\sigma \sim \omega^s$ for large ω. Hence, if $d_\omega^k \widehat{\psi} \in L^1(I\!R)$ so is $d_\omega^k \widehat{\theta}$. Application of Theorem 5 shows the decay rate (3.10). The same arguments apply to η.

Switching to the homogeneous operator with $\dot{\sigma}(0) = 0$ may produce a singularity when dividing by the symbol. As $\widehat{\phi}(0) = 1$, the function η can not be constructed in a classical sense. In other words, the equation $\dot{L}\eta = \phi$ can not be solved for the rhs. ϕ. This is different for $\dot{L}\mu = \psi$. In Fourier space (3.8) reads

$$d_\omega^l \, \widehat{\psi}(\omega) \mid_{\omega=0} \; = 0 \quad , \qquad l = 0, \ldots, M \tag{3.11}$$

As $M \geq s$, the expression $\widehat{\theta} = \widehat{\psi}/\overline{\sigma}$ still has a zero at $\omega = 0$. Therefore $\widehat{\theta}$ and its derivatives exist and remain integrable close to the origin also for the homogeneous case. For large ω the situation is the same as before. □

Theorem 6 has been formulated for the scale $j = 0$. Due to the rescaling property (2.1) for the functions $\psi_{j,i}$ it holds for all j. Inequality (3.10) is just modified by supplementary factors 2^{js} or 2^{-js} in the constants and rescaling of x by 2^j. Other properties can be deduced immediately by similar reasoning.

COROLLARY 2. *Under the conditions of Theorem 6 it can be shown that $\psi, \phi \in H^r$, $\mu, \nu \in H^{r-s}$, and $\theta, \eta \in H^{r+s}$ which holds, apart from η, for the homogeneous case as well. Furthermore, θ and μ have $M + 1$ vanishing moments. In the homogeneous case this number modifies to $M + 1 - s$ and $M + 1 + s$, respecively.*

3.2 Operator–adapted multiresolutions

We now turn to the cardinal Lagrange functions and define the spaces

$$V_{L;J} = \overline{span}\{L\, b_{J,i}\}_i = \overline{span}\{\nu_{J,i}\}_i \tag{3.12}$$

Cardinal functions of these spaces are obtained similarly to the orthogonal case:

THEOREM 7. *Under the conditions of Theorem 6 the spaces $V_{L;J}$ have a cardinal Lagrange function $S_{L;J}$ if*

$$\sum_{k \in \mathbb{Z}} \sigma(\omega + 2^J k) \; \widehat{(b_J)}(\omega + 2^J k) \; \neq 0 \tag{3.13}$$

It is given by

$$\widehat{S_{L;J}}(\omega) = \frac{\sigma(\omega) \; \widehat{b_J}(\omega)}{2^J \sum_{k \in \mathbb{Z}} \sigma(\omega + 2^J k) \; \widehat{(b_J)}(\omega + 2^J k)} \tag{3.14}$$

The same remains true for L replaced by $\dot{L}$.

THEOREM 8. *Under the conditions of Theorem 6 the functions S, S_L, and $S_{\dot{L}}$, if they exist, fulfill the same decay rates in space as ϕ and ψ.*

Proof. $\widehat{S}$ can be obtained through deviding $\widehat{\phi}$ by $\widehat{\phi}^*$, a 1–periodic function. The condition $\mid \widehat{\phi}^* \mid \geq C > 0$ has to be fulfilled for S to exist. Hence, $\mid \widehat{S} \mid \leq \frac{1}{C} \mid \widehat{\phi} \mid$. By construction $\widehat{\phi}^*$ has the same number of derivatives as $\widehat{\phi}$ so that $\widehat{S}$ fulfills the conditions (3.7) and therefore the assertion.
$\widehat{S_L}$ is obtained as $\widehat{S}$ replacing $\widehat{\phi}$ by $\widehat{\nu}$. Using Theorem 6 the above remarks apply identically to $\widehat{S_L}$ and $\widehat{S_{\dot{L}}}$. □

It can be shown that the sets $\{2^{-sj}\mu_{j,i}\}, \{2^{sj}\theta_{j,i}\}$, and $\{2^{-sj}\nu_{j,i}\}$ form Riesz bases of the spaces they generate [FS94], [Pon94]. Considering the homogeneous case we have seen that an algorithm involving the functions $\eta_{j,i}$ would not be practical for large j. Ponenti [Pon94] points out that with increasing j these functions more and more tend to the Greens function of the (inhomogeneous) operator. The common shape for all j destroys the essential zooming–in property. Hence, the functions $\{2^{sj}\eta_{j,i}\}$ do not form a Riesz basis in the limit $j \to \infty$ [Pon94]. This important observation triggered the construction in the cited reference where the unknown u in (3.1) is developed in terms of $\theta_{j,i}$ (and not in terms of $\psi_{j,i}$ as below). To avoid the use of the unstable set $\eta_{J,i}$ a modified basis is constructed by means of some finite difference operator compensating the singularity in Fourier space. This makes the construction rather complicated. Furthermore, the projection step depends on this filter and is not obvious.

The present algorithm has been developed independently from [Pon94]. It is different in the following sense. We do not assume $u \in H^{r+s}$, as with the representation in terms of $\theta_{j,i}$, but rather $u \in H^r$ and approximate the unknown u in (3.1) by some $u_J \in V_J$ [LT90]

$$u_J(x) = \sum_i c_{0,i}\ \phi_{0,i}(x) + \sum_{j=0}^{J-1} \sum_i d_{j,i}\ \psi_{j,i}(x) \tag{3.15}$$

The right hand side f is then approximated accordingly by $f_{L;J} \in V_{L;J}$. With the functions defined above

$$f_{L;J}(x) = \sum_i \langle f, \eta_{J,i}\rangle\ \nu_{J,i}(x) = \sum_i \langle f, \eta_{0,i}\rangle\ \nu_{0,i}(x) + \sum_{j=0}^{J-1} \sum_i \langle f, \theta_{j,i}\rangle\ \mu_{j,i}(x) \tag{3.16}$$

Inserting (3.15), (3.16) in (3.1) and applying a Petrov-Galerkin method with test functions $\{\eta_{0,i}, \theta_{j,i}\}$ shows that having computed the rightmost term of (3.16) the solution u_J is obtained with $c_{0,i} = \langle f, \eta_{0,i}\rangle$, $d_{j,i} = \langle f, \theta_{j,i}\rangle$ in (3.15). In order to determine these coefficients we use the representation of $f_{L;J}$ in terms of the cardinal Lagrange function $S_{L;J}$ of $V_{L;J}$ analogeously to (2.6)

$$f_{L;J}(x) = \sum_i f(\frac{i}{2^J})\ S_{L;J}(x - \frac{i}{2^J}) \tag{3.17}$$

The task then is to accomplish a basis transform from $\{S_{L;J,i}\}$ to $\{\nu_{0,i}, \mu_{j,i}\}$ when f is given at the required grid points. Due to Theorem 8, the limit $j \to \infty$ does not constitute a problem in the construction. Of course, the sums of $\phi_{0,i}$ and $\nu_{0,i}$ in (3.15) and (3.16) can be replaced by linear combinations of $S_{0,i}$ and $S_{L;0,i}$, respectively. This avoids another type of filters.

3.3 Adaptive discretization of an ODE

The biorthogonal basis is now used in the adaptive algorithm of the previous section replacing $S_{J,m}$ with $S_{L;J,m}$ and D^j_m with

$$D^j_{L;m} = \langle S_{L;j,m} \ , \ \theta_{j-1,0} \ \rangle \tag{3.18}$$

One can prove that this filter fulfills analogeous relations as D^j apart from scale invariance. Its decay is determined by Theorems 6 and 8. Another reasoning is illustrative and more direct. It uses the equivalent of Theorem 5 for the Fourier transform $\widehat{f^*}(\omega), \omega \in \mathbb{T}$ (see Appendix).

THEOREM 9. *Under the conditions of Theorem 7 the filter $D^j_{L;m}$ has the same decay with m as D^j_m.*

Proof. Inserting (3.14) and the definition of $\theta_{j,i}$ (3.2) in (3.18) leads to cancellation of the symbol σ and

$$D^j_{L;m} = \int_{\mathbb{T}} \frac{\widehat{b_{j,0}}(\omega)\ \overline{\widehat{\psi_{j-1,0}}(\omega)}\ e^{-2\pi i m\omega}}{2^J \sum_{k\in\mathbb{Z}} \sigma(\omega + 2^J k)\ \overline{(\widehat{b_J})}(\omega + 2^J k)}\, d\omega \tag{3.19}$$

The denominator is a smooth non–zero bounded $2\pi-$periodic function which does not alter the decay properties in physical space. Without this factor the remainder is D^j_m. In [Mey90] a similar argument is applied to the orthonormalization procedure for the classical wavelets. □

We now obtain the following algorithm for the adaptive solution of (3.1):

Algorithm 3: Operator–adapted decomposition

given index set $\Lambda_d \subset \Lambda_J = \{(j,i)|\ j = 0, \ldots, J-1,\ i \in \mathbb{Z}\}$ for the amplitudes $d_{j,i}$ of a lacunary wavelet basis in V_J with some $J \in \mathbb{N}_0$,
a method to evaluate f.

step 0 Compute $D^j_L,\ \mu_{j,0},\ j = 0, \ldots, J$ where $J-1$ is the finest scale in Λ_d.
Truncate these in space according to a given precision.

step 1 Determine the index set Λ_x of points $x_{j,i}$ required in the subsequent quadratures. Require the r.h.s. at these points

$$f_J(x_{j,i}) = f(x_{j.i}) \quad , \qquad (j,i) \in \Lambda_x \tag{3.20}$$

Set $j = J$.

step 2

$$d_{j-1,k} = \sum_{(j,i)\in\Lambda_x} f_j(x_{j,i})\ D^j_{L;i-2k}\ , \qquad (j-1,k) \in \Lambda_d \tag{3.21}$$

step 3

$$f_{j-1}(x_{j-1,i}) = f_j(x_{j,2i})\ - \sum_{(j-1,k)\in\Lambda_d} d_{j-1,k}\ \mu_{j-1,k}(x_{j-1,i})\ , \qquad (j-1,i) \in \Lambda_x \tag{3.22}$$

iterate step 2 and step 3 down to $j = 0$.

final step compute $c_{0,i}$ by the filter $I^j_{L;n} = \langle S_{L;j,n}, \eta_{j,0}\rangle$ with $j = 0$, analogeous to (2.8).

In short, the proposed algorithm for the solution of an ODE (3.1) reads as follows: given the values of the rhs. at an appropriate set of points, Algorithm 3 is employed to determine the coefficients in the development (3.15) of the solution u. The value of the solution at a point of the grid is then obtained by Algorithm 2. Hence we employ a vaguelette–decomposition and a wavelet–reconstruction to solve (3.1). This algorithm has been implemented in a periodized version which is discussed in the following section. Observe that when the filters applied in both steps are not truncated and the entire set of basis functions is used, the method is exactly equivalent to a collocation algorithm on the grid $\{x_{J,i}\}_i$. The inversion of a linear system is replaced by the application of filters into which the inverse of the operator has been incorporated. As soon as these are truncated this yields a method which is neither a Galerkin nor a collocation method but a hybrid one. It relies on both, the localization in space and frequency as well as the orthogonality of the wavelets.

4 Transition to periodic multiresolutions

This section serves to detail some implementational aspects. In particular it gives a comprehensive understanding of what sometimes is just subsumed by the term periodization.

4.1 Mapping from the real line to the circle

Starting from a MRA on the real line, a MRA on the circle $\mathbb{T}$ can be constructed through the projection

$$\widetilde{f}(x) = \sum_{n\in\mathbb{Z}} f(x+n) \tag{4.1}$$

from $L^2(\mathbb{R})$ onto $L^2(\mathbb{T})$ [PB89, Mey90]. In Fourier space it reads

$$\widehat{\widetilde{f}}(n) = \widehat{f}(n) \quad , \qquad n \in \mathbb{Z} \tag{4.2}$$

(see Appendix). This generates the periodic analogues $\widetilde{b_{j,k}}, \widetilde{\phi_{j,k}}, \widetilde{\psi_{j,k}}$ of the functions $b_{j,k}, \phi_{j,k}, \psi_{j,k}$ and the periodic MRA of the spaces $\widetilde{V_j} = span\{\widetilde{b_{ji}}\}_{i=0,\ldots,2^j-1}$, $j \in \mathbb{N}_0$. The index range is due to the periodicity $\widetilde{f_{j,i}} = \widetilde{f_{j,i+k\,2^j}}$, $(k \in \mathbb{Z})$ introduced by (4.1). It carries over to all filters and functions in $L^2(\mathbb{T})$ below. By construction the orthogonality between shift invariant functions is preserved under (4.1). Furthermore $\widetilde{\phi_{j,k}} = 1$ for $j \leq 0$ as the functions $\{\phi_{j,i}\}_i$ constitute a partition of unity and $\widetilde{S_{0,0}} = \widetilde{\phi_{0,0}}$ for the same reason. Denoting this function $\widetilde{\psi_{-1,0}}$ for brevity, any $\widetilde{f_J} \in \widetilde{V_J}$ can then be written as

$$\widetilde{f_J}(x) \;=\; \sum_{j=-1}^{J-1} \sum_{k=0}^{\lceil 2^j-1 \rceil} d_{j,k}\; \widetilde{\psi_{j,k}}(x) \tag{4.3}$$

In the periodic setting the indices in scale do no longer refer to an afine transform such as (2.1) but rather to applying (2.1) for the non–periodic counterpart followed by (4.1). A result is that functions and filters are related through recurrence relations in Fourier space [PB89]. In other words they are obtained from their non–periodic counterparts through coarser and coarser sampling for decreasing j. The values of $\widetilde{H}^j_n = \langle \widetilde{\phi_{j,n}}, \widetilde{\phi_{j-1,0}} \rangle, n = 0, \ldots, 2^j - 1$, for example can be obtained by

$$(\widehat{\widetilde{H}^j})_k = 2^{-j} \widehat{H}^*(\frac{k}{2^j}) \quad , \qquad k = 0, \ldots, 2^j - 1 \tag{4.4}$$

with $\widehat{H}^*$ from (2.4). Using the mapping (4.1) a cardinal Lagrange function is readily obtained similarly to Theorem 1:

THEOREM 10. *Let b fulfil the requirements of Theorem 1 and let $\widetilde{V_j} = span\{\widetilde{b_{j,i}}\}_{i=0,\ldots,2^j-1}$ ($j \in \mathbb{N}_0$) be defined through (2.1), (4.1). Then a cardinal Lagrange function of $\widetilde{V_j}$ exists and is given by*

$$\widehat{\widetilde{S_j}}(n) = \frac{\widehat{\widetilde{b}}_j(n)}{2^j\, (\widehat{\widetilde{b_j}})_n} \quad , \qquad n \in \mathbb{Z} \tag{4.5}$$

Proof. Since V_j is spanned by shifts of S_j, $\widetilde{V_j}$ is spanned by shifts of $\sum_{k\in\mathbb{Z}} S_j(x+k)$. Obviously, the interpolation property is preserved through periodization so that this sum indeed is again a cardinal Lagrange function of $\widetilde{V_j}$ and therefore defines $\widetilde{S_j}$ due to its uniqueness. Using (2.9), (4.2), and (8.4) yields (4.5). Nonvanishing denominator is ensured by the condition on b. □

4.2 Implementation for spline– and Meyer wavelets

The required filters in the algorithms devised above have to be determined in a preprocessing step. Throughout, we first compute the exact values and only subsequently

truncate the filters with respect to their length. We employ multiresolutions of Battle-Lemarié spline wavelets of even order and Meyer wavelets. As both have non-compact support, a few remarks are appropriate.

In the present cases the filters H, G, I, D, D_L for the non–periodic MRAs are given explicitly in Fourier space. Recall that these expressions are 1–periodic functions in ω (cf. equation (2.4)). Hence, no error is introduced through the periodization by replacing ω with $k/2^j$. This property is not shared by the functions ϕ, ψ, S, μ, etc., they can be defined in Fourier space but have large or unbounded support in ω. Therefore the exact values of these functions have to be deduced from the filters. The values $\widetilde{\psi_{J-1,0}}(x_{J,i})$ for example are computed by a standard inverse wavelet transform having initialized with $d_{ji} = \delta_{j,J-1}\,\delta_{i,0}$. In the particular case of Meyer wavelets the compact support in Fourier space can be used to alternatively obtain the function's values by a DFT of appropriate length since the sum in (8.6) contains at most two entries. As the symbol σ does not alter the support in frequency space this holds for $\widetilde{\theta}, \widetilde{\mu}, \widetilde{S_L}$ as well.

For spline wavelets the procedure is more involved. We first compute an interpolation function in the non-periodic case. Thereto, $L\,b_j = 2^{j/2} L N_m(2^j x)$ with N_m designating the B-spline of m–th order. Relating $\widehat{N_m}^*$ to the derivative of the cotangent function [Chu92], formulae for $\widehat{Lb_j}^*$ are deduced to express $\widehat{S_{L;j}}(\omega)$. This defines the operator adapted interpolation filter $\widehat{I_L^j}^*(\omega)$. Due to the linearity of the operator L the functions μ, ν fulfil the same refinement equation as ψ, ϕ. Hence, $\widehat{G_L^j}^* = \widehat{G^j}^*$. The resulting expression for $\widehat{D_L^j}^*(\omega)$ is then sampled to accomplish the transfer to the periodic setting. Subsequently, the values of $\widetilde{\mu_{j,0}}$ at grid points are generated by the filters as described above.

Finally note that different MRAs can of course be used to start from. However, we conjecture that a construction in which all the required filters are of compact support can not be obtained. Daubechies wavelets for example have compact support, but the related cardinal function has not. The autocorrelation of the Daubechies scaling functions does furnish compactly supported cardinal functions. However, these MRAs do not permit compactly supported orthogonal wavelets. Also the construction of [DW93] of compactly supported operato–adapted wavelets does not lead to full (bi–)orthogonality of the basis. Further research is required to elucidate this question.

5 Two–dimensional adaptive algorithm

The use of an additional Fourier series for the discretization of a two–dimensional problem as in [FS94] is straightforward and skipped here. Instead, we have extended the present method to two–dimensional tensorproduct MRAs [Mey90]. In this framework the solution u is developed as

$$u_J(x,y) = \sum_{k_x}\sum_{k_y} c_{0,k_x,k_y}\;\phi_{0,k_x,k_y}(x,y) \quad + \quad \sum_{j=0}^{J-1}\sum_{k_x}\sum_{k_y}\sum_{\varepsilon=1}^{3} d^{\varepsilon}_{j,k_x,k_y}\;\psi^{\varepsilon}_{j,k_x,k_y}(x,y) \quad (5.1)$$

with

$$\phi_{j,k_x,k_y}(x,y) = \phi_{j,k_x}(x)\ \phi_{j,k_y}(y) \tag{5.2}$$

and

$$\psi^{\varepsilon}_{j,k_x,k_y}(x,y) = \begin{cases} \psi_{j,k_x}(x)\ \phi_{j,k_y}(y) & ;\ \varepsilon = 1 \\ \phi_{j,k_x}(x)\ \psi_{j,k_y}(y) & ;\ \varepsilon = 2 \\ \psi_{j,k_x}(x)\ \psi_{j,k_y}(y) & ;\ \varepsilon = 3 \end{cases} \tag{5.3}$$

The method previously described for the solution of an ODE in space can now be applied analogeously to the discretization of a PDE in two dimensions. Periodicity is accounted for by the technique of section 4.1.

6 Applications and numerical results

6.1 Truncation of filters

As a preliminary step the precision of the above wavelet transform has been investigated for different truncations. Setting $f = \psi_{j,0}$, $(j = -1, \ldots, J-1)$ all coefficients are computed up to $J-1$. The left part of Table 1 reports

$$E_1 = \max_{jkm} \{ |\ fo\langle \psi_{j,0}, \psi_{k,m} \rangle_Q\ -\ \delta_{j,k}\ \delta_{0,m}\ | \} \tag{6.1}$$

where the index Q of the scalar product denotes its evaluation by the described recursive quadrature of Algorithm 1. In an analogeous way the inverse transform has been tested. The error E_2 is defined similarly to (6.1) replacing $\psi_{j,0}$ with the function generated by the inverse transform and $\langle \cdot, \cdot \rangle_Q$ by the exact scalar product. This is realized in starting from $d_{j,0} = 1$ for one particular value of j and all other coefficients zero. An inverse transform with truncation and a subsequent exact forward transform without truncation are then executed.

	E_1			E_2		
K	Meyer	$m=6$	$m=4$	Meyer	$m=6$	$m=4$
full grid	8.7 E-14	5.7 E-14	3.4 E-14	5.5 E-14	7.7 E-14	5.7 E-14
40	2.7 E-5	3.8 E-5	5.6 E-7	8.9 E-6	1.4 E-5	2.2 E-7
30	1.6 E-4	4.1 E-4	1.8 E-5	9.1 E-5	1.2 E-4	5.7 E-6
20	8.6 E-4	4.5 E-3	5.3 E-4	6.3 E-4	1.2 E-3	1.6 E-4

Table 1. Projection error E_1 of Algorithm 1 and E_2 of Algorithm 2 for Meyer wavelets, cubic spline wavelets ($m = 4$) and quintic spline wavelets ($m = 6$). K denotes the number of points from the center of D^j, S_j and $\psi_{j,i}$ at which summations are stopped, respectively. Finest scale is $J = 10$.

6.2 Helmholtz problem

A practically relevant example for the presented method is a Helmholtz–type equation arising e.g. from a semi–implicit time discretization of parabolic equations as applied below. Hence, for the remainder we set

$$L = \lambda \; - \; \partial_{xx} \quad , \qquad \lambda \in I\!R^{>0} \tag{6.2}$$

i.e. $\sigma(\xi) = \lambda + 4\pi^2\xi^2, s = 2$. In the sample computations $\lambda = 150$ has been used corresponding to the time stepping for the PDE below.

Similar to Table 1 we first consider the influence of the truncation on the orthogonality of the basis functions in the operator–adapted case. Some examples are assembled in Table 2. The error E_3 is defined as in (6.1) replacing $\psi_{j,0}$ by $\mu_{j,0}$ and $\psi_{k,m}$ by $\theta_{k,m}$ (unfortunately, comparison to a similar table in [FS94] is not possible for implementational reasons). The level of round off errors is given by the first line. The precision achieved with truncated filters increases if these have stronger decay, i.e. in case of low regularity of the basis.

K_D, K_μ	Meyer	$m = 6$	$m = 4$
full grid	1.5 E-12	2.8 E-12	3.5 E-12
60, 60	3.5 E-5	1.1 E-5	3.0 E-8
40, 40	3.5 E-4	8.5 E-4	2.2 E-5
30, 30	1.6 E-3	8.9 E-3	6.1 E-4
80, 60	1.6 E-5	7.7 E-7	2.6 E-9
40, 30	3.4 E-4	1.1 E-3	5.3 E-5

Table 2. Projection error E_3 of Algorithm 3 for Meyer wavelets and quintic and cubic spline wavelets. K_D, K_μ denote the number of points from the center of $D_{L;j}$ and $\mu_{j,i}$ at which quadrature and summation are stopped, respectively. Finest scale is $J = 10$.

Next, we report the precision obtained for the solution of the Helmholtz equation (3.1), (6.2), with a right hand side such that the exact solution is

$$u_{ex}(x) = e^{-\gamma^2(x-\frac{1}{2})^2} \qquad ; \qquad \gamma^2 = 16000 \tag{6.3}$$

Figure 1 displays the resulting L^2–approximation error when computing all wavelet amplitudes of the solution, the L^∞–error behaves analogeously. As stated before, the use of untruncated filters results in a pure collocation method the convergence rate of which is determined by the regularity of the basis functions. With truncated filters the approximation can not be improved beyond the level induced by the defect in orthogonality. Hence, the error tends to a constant with increasing J when this level is reached. Observe that the values in Figure 1 nicely correspond to those of Table 2 (in general a multiplicative factor appears). Furthermore, the result with Meyer wavelets can be

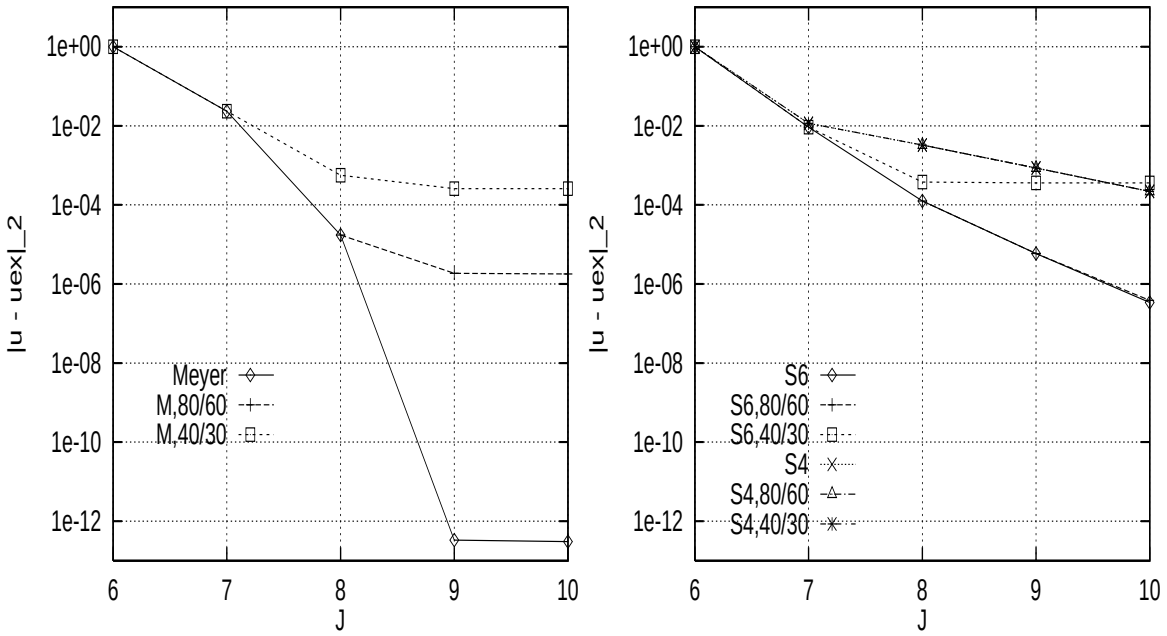

FIG. 1. L^2–error of the Helmholtz problem solved with Algorithm 3 and different basic multiresolutions. LEFT: Meyer wavelets. RIGHT: quintic and cubic spline wavelets (all curves of the latter are virtually identical).

compared to Fig.7 of [FS94]. They exhibit an improvement by roughly two orders of magnitude or, in other terms, half the filter size for the same precision.

Due to the interpolatory approach it is also possible now to use spline wavelets in the solution procedure. The results in the right part of Figure 1 support the above interpretation. For $m = 6$ only the stronger truncation influences the accuracy whereas with $m = 4$ the filters could still be shortened without loosing considerable precision with respect to the exact result on the respective grids.

To assess the amount of adaptivity which is possible by the approach, Table 3 finally displays the number N_ϵ of coefficients which are larger in absolute value than the truncation error $\epsilon = |u - u_{ex}|_2$ with the full basis depicted in Figure 1. Employing only these coefficients in an adaptive computation would lead to drastic savings at the expense of an $O(\epsilon)$–error.

In summary, the proposed method permits an $h - p$–like strategy. On one hand there are very regular basis functions and longer filters leading to higher precision on large scales. On the other hand there are bases with low regularity which lead to shorter filters but steeper cones in the index space arround singularities or almost–singularities of the solution. The actual choice has to depend on the convergence rate in the non-truncated case and the size of the filters which is needed to maintain the required precision.

J	7	8	9	10
M full	18	98	508	508
M 80,60	18	98	146	146
M 40,30	18	56	66	66
S6 full	18	74	116	148
S6 80,60	18	74	116	148
S6 40,30	18	56	58	58
S4 full	12	26	38	58
S4 80,60	12	26	38	58
S4 40,30	12	26	38	58

TABLE 3. Number N_ϵ of significant amplitudes in the computations of Figure 1 (see text).

6.3 Adaptive solution of a nonlinear parabolic PDE

The above discretization has been devised for the adaptive solution of a PDE with evaluation of nonlinear terms in physical space. As an example it is applied here to a reaction diffusion equation originating from laminar premixed combustion and amply discussed e.g. in [DH92]. In the one–dimensional case with unitary Lewis number the equations simplify for certain initial and boundary conditions to

$$\begin{aligned} \partial_t \tilde{T} \; - \; \frac{1}{L_x^2} \partial_{xx} \tilde{T} \;\; &= \;\; \tilde{\omega} \; + \; \frac{1}{L_x^2} d_{xx} s \quad , \qquad x \in \mathbb{T} \\ \tilde{\omega} \;\; &= \;\; \frac{\beta^2}{2} (1 - \tilde{T} - s) \; e^{\frac{\beta(\tilde{T}+s-1)}{1+\alpha(\tilde{T}+s-1)}} \end{aligned} \tag{6.4}$$

The smooth function $s(x)$ is used for periodization [DH92], $\tilde{T}$ and $\tilde{\omega}$ are the (periodic) temperature perturbation and the reaction rate, respectively, and L_x is the physical size of the domain. Suitable initial conditions result in a steadily propagating front. The stiffness of the problem is governed by β as increasing its value reduces the size of the reaction zone, i.e. the region where $\tilde{\omega} >> 0$. We employ the second order semi–implicit time scheme and the adaptive selection procedure for the wavelet coefficients of [FS94]. The solution is advanced in time by performing a backward transform of the actual solution to the locally refined grid of quadrature points (Algorithm 2), evolution of the rhs., and finally a decomposition into the operator adapted basis (Algorithm 3) to compute the wavelet amplitudes of the solution of the new time step.

A result is reported in Figure 2. This computation for $L_x = 30$, $\alpha = 0.8$, $\beta = 10$ has been performed with cubic spline wavelets and $\Delta_t = 0.01$, $J = 10$, $\epsilon = 1.e-5$. The adaptive discretization follows the front without problem requiring a number of significant coefficients of about $N_\epsilon = 66$ most of the time. Nevertheless the very sensitive reaction rate is well approximated. With respect to former computations [FS94] the new projection method leads to reduced cpu time (factor of about 4 for this particular setting) and a reduced number of quadrature points. This is particularly advantageous when

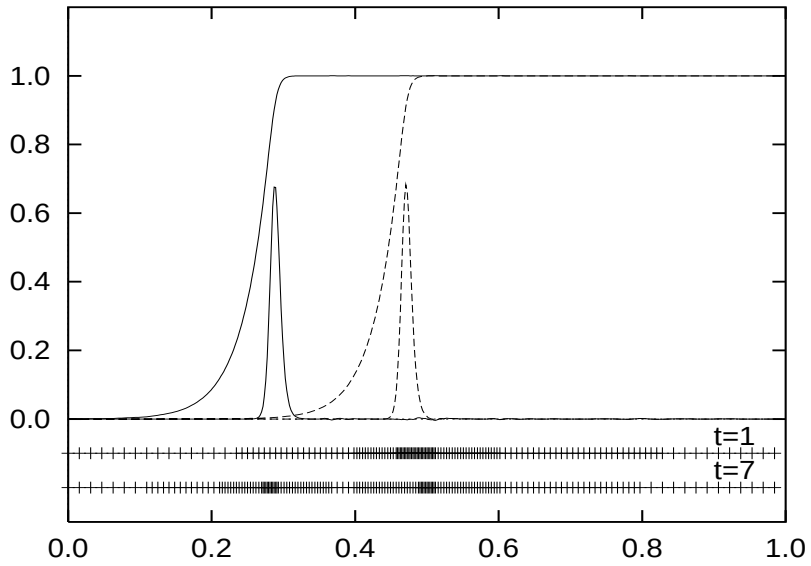

FIG. 2. Physical temperature $T = \tilde{T} + s$ and reaction rate $\tilde{\omega}$ (devided by 2.5 for presentation) versus x for a left–traveling thermodiffusive flame front. The dotted curves correspond to $t = 1$, the continuous ones to $t = 7$. The tics below indicate the centers of the adaptively selected wavelet basis functions involved at the respective times. A number larger than N_ϵ is required by the algorithm employed for the adaptive selection of basis functions. The second cloud for $t = 7$ at $x = 0.5$ is due to the periodizing function $s(x)$.

the evaluation of the rhs is costly.

6.4 Two–dimensional adaptive computation

Figure 3 reports a sample computation for the two–dimensional analogue of (6.4) for $(x, y) \in \mathbb{T} \times \mathbb{T}$ with $s \equiv 0$ and $L_x = L_y = 30$. The initial state is given by an inclined elliptical flame front which then propagates in outward direction. Due to the physical stability of thermodiffusive flames at unitary Lewis number [Siv77] the front relaxes to a circle. This example has been selected as its solution is difficult to resolve e.g. by parametrized mapping techniques.

The left part of the figure shows level lines of the solution at $t = 1$. The right part presents the instantaneous set of adaptively selected coefficients in (5.1). Only these are computed while the remaining ones are set to zero. The algorithm for the determination of the relevant amplitudes in the actual time step is based on proximity relations in scale space. They can be defined similarly to the one–dimensional case. The finest scale in this computation was $J = 7$ yielding 128×128 possible degrees of freedom. At $t = 1$ only 1510 i.e. roughly 10% of them are required to represent the solution with the desired accuracy ($\epsilon = 10^{-5}$). The employed MRA is based on cubic splines. Observe that although the basis functions reflect to some extent the orthogonal coordinate system this does not degrade the adaptive discretization in oblique directions.

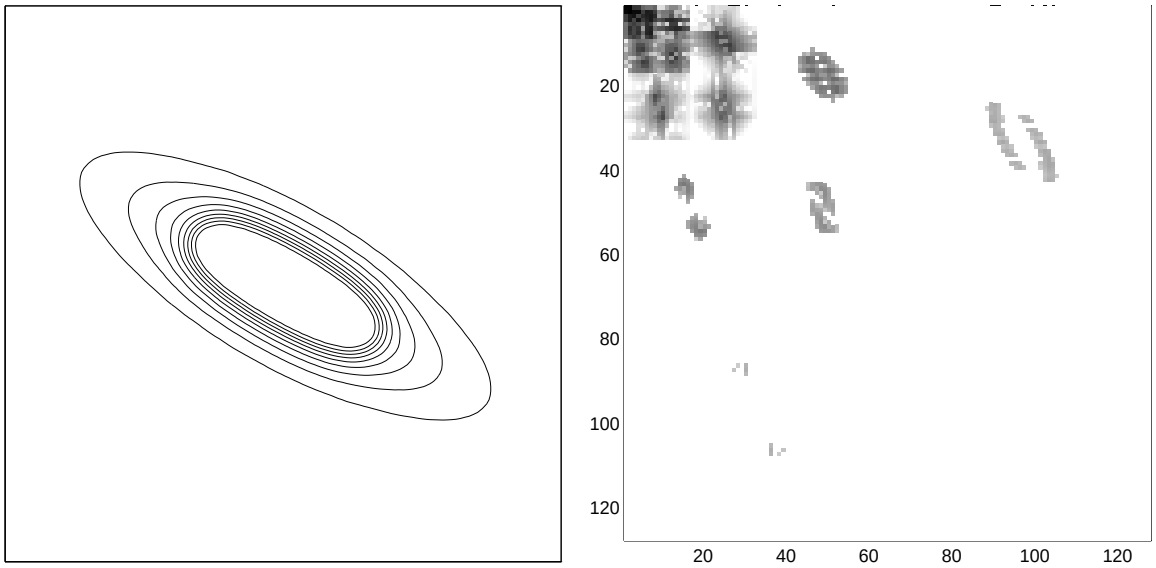

FIG. 3. Computation of an elliptic two–dimensional flame front. LEFT: Level lines of the temperature at $t = 1$. RIGHT: Active coefficients in (5.1) located in the standard way [Dau92, p.315]: $d^{\varepsilon}_{j,k_x,k_y}$ is positioned at $x = 2^j(1 - \delta_{\varepsilon,3}) + k_x$, $y = 2^j(1 - \delta_{\varepsilon,1}) + k_y$.

7 CONCLUSION

The present algorithm is a step towards an atom–like use of wavelet basis functions for the solution of PDEs. We have developed the method in one dimension and have analyzed the resulting filters. The approach has also been extended to a truely two–dimensional fully adaptive wavelet discretization in space. Essential boundary conditions can now be implemented using imbedding strategies as mentioned in the introduction. With respect to earlier work [FS94] the improved methodology results in a clearer presentation, an easier analysis and increased efficiency.

On the other hand it is evident that the employed filters are still unsatisfactory as they do not have compact support right from the start and have to be truncated. The basic multiresolutions with non–compactly supported cardinal functions are not the only reason for this fact. A further difficulty results from the incorporation of the operator inverse which is related to the Greens function. Its advantage is that no linear system needs to be solved. Other approaches in the literature such as [BCR91], [CP95] start from the representation of the inverse of an operator by means of a wavelet basis (standard or non–standard form) and determine an approximation by cancelling small matrix entries. This operation is similar to the employed truncation of filters. Hence, the requirement of truncation is no particularity of the present construction but rather a general feature which, nevertheless, would be convenient to overcome. In [JS93] diagonalization for the Helmholtz operator is obtained at the price of non–constant weight in the scalar product and $O(h^2)$ convergence of the final algorithm and a low order projection. Future research will be concerned with the construction of improved bases for the presented algorithm.

8 Appendix: Definition of the employed Fourier transforms

The employed Fourier transforms of square integrable functions are

$$\widehat{f}(\omega) = \int_{I\!R} f(x)\, e^{-2\pi i\omega x}\, dx \quad , \qquad \omega \in I\!R \tag{8.1}$$

$$\widehat{\widetilde{f}}(n) = \int_{I\!T} \widetilde{f}(x)\, e^{-2\pi i n x}\, dx \quad , \qquad n \in Z\!\!Z \tag{8.2}$$

in the non-periodic and the periodic case, respectively. The symbol $I\!T$ designates the circle or one–dimensional torus $I\!T = I\!R/Z\!\!Z$. The brackets around $n \in Z\!\!Z$ in (8.2) are motivated by (4.2). They serve to distinguish (8.2) from the discrete Fourier transform (DFT) of length 2^j with some $j \in I\!N_0$ defined by

$$\widehat{\widetilde{f}}_k = \frac{1}{2^j} \sum_{n=0}^{2^j-1} \widetilde{f}(\frac{n}{2^j})\, e^{-2\pi i n k/2^j} \quad , \qquad k = 0, \ldots, 2^j - 1 \tag{8.3}$$

Considering a 1–periodic function $\widetilde{f}$, the coefficients of a DFT with 2^j entries are related to $\widehat{\widetilde{f}}(n)$ through the 'aliasing relation'

$$\widehat{\widetilde{f}}_k = \sum_{z \in Z\!\!Z} \widehat{\widetilde{f}}(k + 2^j z) \quad , \qquad k = 0, \ldots, 2^j - 1 \tag{8.4}$$

Finally, the transform

$$\widehat{f}^*(\omega) = \sum_{n \in Z\!\!Z} f(n)\, e^{-2\pi i\omega n} \quad , \qquad \omega \in I\!T \tag{8.5}$$

is obtained from the sampled values of f. It fulfils

$$\widehat{f}^*(\omega) = \sum_{k \in Z\!\!Z} \widehat{f}(\omega + k) \quad , \qquad \omega \in I\!T \tag{8.6}$$

due to the Poisson summation formula. Eqs. (8.3)–(8.6) remain valid for $k \in Z\!\!Z$, $\omega \in I\!R$, since $\widehat{\widetilde{f}}_k$ and $\widehat{f}^*$ are periodic with period 2^j and 1, respectively.

References

[BCR91] G. Beylkin, R. Coifman, and V. Rokhlin. Fast wavelet transforms and numerical algorithms I. *Comm. Pure Appl. Math.*, 44:141–183, 1991.

[Bey93] G. Beylkin. On the Fast Algorithm for Multiplication of Functions in the Wavelet Basis. In Y. Meyer and S. Roques, editors, *Progress in Wavelet Analysis and Applications, Proceedings of the International Conference Wavelets and Applications, Toulouse, 1992*, pages 259–273. Editions Frontiers, 1993.

[BFF95] R. Brand, W. Freeden, and J. Fröhlich. An Adaptive Hierarchical Approximation Method on the Sphere Using Axisymmetric Locally Supported Basis Functions. Technical Report SC 95–2, Konrad–Zuse–Zentrum für Informationstechnik Berlin, 1995.

[BMP92] E. Bacry, S. Mallat, and G. Papanicolaou. A wavelet based space-time adaptive numerical method for partial differential equations. *Math. Mod. Num. Anal.*, 26:793, 1992.

[BN93] S. Bertoluzza and G. Naldi. Some Remarks on Wavelet Interpolation. Technical Report N. 886, Instituto di Analisi Numerica del CNR, 1993.

[Chu92] C.K. Chui. *An Introduction to Wavelets*. Academic Press, 1992.

[CP95] Ph. Charton and V. Perrier. Factorisation sur bases d'ondelettes du noyau de la chaleur et algorithmes matriciels rapides associés. *C.R.Acad.Sci. Paris, série I*, 320:1013–1018, 1995.

[Dau92] I. Daubechies. *Ten Lectures on wavelets*. SIAM, 1992.

[DH92] B. Denet and P. Haldenwang. Numerical Study of Thermal-Diffusive Instability of Premixed Flames. *Combust. Sci. and Tech.*, 86:199–221, 1992.

[DK92] W. Dahmen and A. Kunoth. Multilevel preconditioning. *Numer. Math.*, 63:315–344, 1992.

[DLY89] P. Deuflhard, P. Leinen, and H. Yserentant. Concepts of an Adaptive Hierarchical Finite Element Code. *IMPACT Comput. Sci. Engrg.* , 1:3–35, 1989.

[DW93] S. Dahlke and I. Weinreich. Wavelet-Galerkin methods, an adapted biorthogonal wavelet basis. *Constr. Approx.*, 9:237–262, 1993.

[EOZ94] B. Engquist, S. Osher, and S. Zhong. Fast wavelet based algorithms for linear evolution equations. *SIAM J. Sci. Comput.*, 15:755–775, 1994.

[FS94] J. Fröhlich and K. Schneider. An adaptive wavelet Galerkin algorithm for one– and two-dimensional flame computations. *Eur. J. Mech., B/Fluids*, 13:439–471, 1994.

[GRWZ93] R. Glowinski, A. Rieder, R.O. Wells, and X. Zou. A Wavelet Multigrid Preconditioner for Dirichlet Boundary Value Problems in General Domains. preprint, 1993.

[Jaf89] S. Jaffard. Exposants de Hölder en des points donnés et coefficients d'ondelettes. *C.R.Acad.Sci. Paris I*, 308:79–81, 1989.

[Jaf92] S. Jaffard. Wavelet Methods for Fast Resolution of Elliptic Problems. *SIAM J. Numer. Anal.*, 29:965–986, 1992.

[JS93] B. Jawerth and W. Sweldens. Wavelet multiresolution analyses adapted for the fast solution of boundary value ordinary differential equations. In T.A. Manteuffel N.D. Melson and S.F. McCormick, editors, *Sixth Copper Mountain Conference on Multigrid Methods*, pages 259–273, 1993.

[JS94] B. Jawerth and W. Sweldens. An Overview of Wavelet Based Multiresolution Analyses. *SIAM Rev.*, 36:377–412, 1994.

[Lem91] P.G. Lemarié. Fonctions a support compact dans les analyses multi–résolutions. *Rev. Math. Iberoamericana*, 7:157–182, 1991.

[LT90] J. Liandrat and Ph. Tchamitchian. Resolution of the 1D regularized Burgers equation using a spatial wavelet approximation algorithm and numerical results. Technical report, ICASE, 1990.

[Mey90] Y. Meyer. *Ondelettes et Opérateurs I/II*. Herman, 1990.

[MPR91] Y. Maday, V. Perrier, and J.Ch. Ravel. Adaptivité dynamique sur bases d'ondelettes pour l'approximation d'équations aux derivées partielles. *C.R.Acad.Sci. Paris I*, 312:405–410, 1991.

[MR92] Y. Maday and J.Ch. Ravel. Adaptivité par ondelettes: conditions aux limites et dimensions supérieures. *C.R.Acad.Sci. Paris I*, 315:85–90, 1992.

[PB89] V. Perrier and C. Basdevant. La décomposition en ondelettes périodiques, un outil pour l'analyse de champs inhomogènes. Théorie et algorithmes. *Rech. Aérosp.*, 1989-3:53–67, 1989.

[Pla92] F. Plantevin. PhD thesis, University Aix–Marseille I, 1992.

[Pon94] P. Ponenti. *Algorithmes en ondelettes pour la résolution d'équations aux dérivées partielles*. PhD thesis, University Aix–Marseille I, 1994.

[QW93] Z. Qian and J. Weiss. Wavelets and the Numerical solution of partial differential equations. *J. Comp. Phys.*, 106:155–175, 1993.

[Sch69] I.J. Schoenberg. Cardinal Interpolation and Spline Functions. *J. Approx. Theory*, 2:167, 1969.

[Siv77] G.I. Sivashinski. Nonlinear Analysis of Hydrodynamic Instability in a Flame I: Derivation of Basic Equations. *Acta Astronaut*, 4:1177–1206, 1977.

[SP94] W. Sweldens and R. Piessens. Quadrature formulae and asymptotic error expansions for wavelet approximations of smooth functions. *SIAM J. Numer. Anal.*, 31:1240–1264, 1994.

[SW71] E.M. Stein and G. Weiss. *Fourier analysis on Eukledian spaces*. Princeton University Press, 1971.

[Swe94] W. Sweldens. The lifting scheme: A custom-design construction of biorthogonal wavelets. Technical Report 1994:7, IMI, Dep. of Math., Univ. of South Carolina, 1994.

[Tch87] Ph. Tchamitchian. Biorthogonalité et théorie des opérateurs. *Revista Matemática Iberoamericana*, 3, 1987.

[VPS95] O.V. Vasilyev, S. Paolucci, and M. Sen. A Mulitlevel Wavelet Collocation Method for Solving Partial Differential Equations in a Finite Domain. *J. Comp. Phys.*, 120:33–47, 1995.

[Wal92] G. Walter. A sampling theorem for wavelet subspaces. *IEEE Trans. Inform. Theory*, 38:881–884, 1992.